Electronic supplementary information

Electrochemical Contact Modification with MoO_3: a Strategy to Enhance Performance of p-Type Organic Thin-Film Transistors

Xuanhe Li,[†a] Yonghua Zhou,[†a] Zhenxin Yang,[a,b] Fushun Li,[a] Jiale Su,[a] Dengke Wang,[a] Zhenghong Lu[a] and Qiang Zhu[*a]

[a] Key Laboratory of Yunnan Provincial Higher Education Institutions for Optoelectronics Device Engineering, School of Physics and Astronomy, Yunnan University, Kunming 650504, China.

[b] Institute for Engineering Medicine, Kunming Medical University Kunming, Yunnan 650500, China

† Xuanhe Li and Yonghua Zhou contributed equally to this work.

* Corresponding author (email: qiangzhu@ynu.edu.cn, yangzhenxin@kmmu.edu.cn)

1. Experimental Methods

1.1 Device Fabrication

The fabrication of all OFETs was conducted on heavily doped silicon wafers with a 300 nm SiO_2 layer. Prior to device fabrication, the wafers were subjected to sequential ultrasonic cleaning with acetone, methanol, and deionized, followed by ultraviolet ozone treatment for 30 min. The Au-based source-drain electrodes, with a width of 5000 μm and a length of 50 μm, were patterned onto the cleaned wafers by vacuum thermal evaporation at a rate of 0.3 Å s^{-1} using an interdigital mask, which consisted of a 5 nm Cr layer followed by a 30 nm Au layer. The Au-electrode patterned wafers were sequentially subjected to ultrasonic cleaning with acetone, methanol, and deionized water, followed by baking in air at 100 °C for 10 min and ultraviolet ozone treatment for 30 min. The bottom-gate bottom-contact (BGBC) structure was employed to the OFET fabrication (**Figure 1a**), wherein an organic semiconductor (OSC) film was directly deposited onto the cleaned Au-electrode patterned wafers using the solution spin-coating method at a rate of 1500 rpm for 60 s, resulting in the device being referred to as BGBC/Au OFET. The spin-coating process involved the preparation of two solutions containing distinct OSCs. One solution consisted of 10 mg of Rubrene blended with Polystyrene at a weight ratio of 8:1, dissolved in 1 mL of 1,2-dichlorobenzene. The other solution contained 10 mg of TIPS-pentacene dissolved in 1 mL of 1,2-dichlorobenzene. All the chemicals used were obtained from Sigma. All obtained devices underwent annealing at a temperature of 170 °C for 20 min and were then encapsulated with glass within a N_2-filled glovebox.

Furthermore, the BGBC devices were fabricated using physical vapor deposition (PVD) method to form MoO_3-modified Au (PVD-MoO_3@Au) electrodes, denoted as

BGBC/PVD-MoO_3@Au OFET. A 30 nm Au layer and a 40 nm MoO_3 layer were sequentially deposited onto the cleaned wafers through the mask at an evaporation rate of 0.3 Å s^{-1}, followed by coating with an OSC films for the fabrication of OFETs with the MoO_3 modified electrodes (**Figure 1b**). For comparative study, the bottom-gate top-contact (BGTC) OFETs were fabricated by sequentially spin-coating the OSC film and depositing patterned MoO_3 and Au electrodes under identical aforementioned conditions (**Figure 1c**).

Moreover, the Au electrodes of the BGBC devices were modified with MoO_3 using electrochemical deposition (ECD) method (**Figure 1d**), in which the electrodes were referred to as ECD-MoO_3@Au and the obtained device were denoted as BGBC/ECD-MoO_3@Au OFET. The electrochemical method utilized an aqueous electrolyte of ammonium molybdate (0.03 mol/L) in deionized water, adjusting to pH 3 by adding sulfuric acid. The different thickness of MoO_3 layers were electrochemically deposited onto oneside of electrodes by doping the electrolyte onto the electrodes and applying a bias voltage of –2 V for 10, 30, 60, 120, and 200 seconds, respectively. The resulted wafers with ECD-MoO_3@Au electrodes were sequentially cleaned with acetone, methanol, and deionized water for 3 min using ultrasonic cleaning, followed by baking in air at 100 °C for 10 min and ultraviolet ozone treatment for 30 min. The obtained wafers with ECD-MoO_3@Au electrodes were followed by coating with an OSC films under identical aforementioned conditions.

To compare the advancements of the ECD method in OFET fabrication, other low-temperature methods based on sol-gel spin-coating [S1] and spray pyrolysis [S2] were employed to modify the Au electrodes. These methods involved depositing MoO_3 layers onto Au-electrode patterned wafers for the fabrication of BGBC devices. For the

sol-gel spin-coating method, the MoO_3 sol-gel solution was prepared by dissolving 0.25 g of ammonium molybdate in 10 mL of deionized water and continuously stirring it to obtain a homogeneous solution. 100 μL of the prepared sol-gel solution was applied to the cleaned Au-electrode patterned wafers and spin-coated at 3000 rpm for 30 s. After the sol-gel coating, the wafers were placed on a hot plate at 100 °C for 10 min to evaporate the solvents. This process was repeated twice to ensure the film uniformity. Finally, the spin-coated films were annealed at 450 °C for 2 h in a muffle furnace in air. For the spray pyrolysis method, the MoO_3 solution was prepared by dissolving 0.19 g of ammonium molybdate in 10 mL of deionized water and continuously stirring the mixture until a homogeneous solution was obtained. Subsequently, the solution was sprayed as a fine mist onto the pre-heated Au-electrode patterned wafers at 450 °C via spray pyrolysis. Nitrogen gas at 0.35 bar was used as the carrier gas, and the solution flow rate is 4 mL min^{-1}. The obtained MoO_3 modified Au-electrode patterned wafers were sequentially cleaned with acetone, methanol, and deionized water for 3 min using ultrasonic cleaning, followed by baking in air at 100 °C for 10 min and ultraviolet ozone treatment for 30 min. The obtained wafers with the MoO_3-modified electrodes were followed by coating with an OSC films under identical aforementioned conditions. Notably, the OSC films coated onto the wafers for device fabrication should undergo annealing at a temperature of 170 °C for 20 min and then encapsulated with glass within a N_2-filled glovebox.

2.2 Device Measurements

The optical images of the electrode patterns and the MoO_3 thin-film layers were observed using an optical microscope (AOSVI M330BD-HD228S). The morphologies

of MoO_3 layers deposited on the Au surface were investigated by a scanning electron microscope (SEM, Nova NanoSEM 450) and an atomic force microscope (AFM, Bruker Multi-Mode 8). The UV-vis absorption spectra of the materials were recorded using ultraviolet-visible spectrophotometer (INESA N4S). The infrared absorption spectra of the materials were measured using a Fourier transform infrared (FTIR) spectrometer (Thermo Scientific Nicolet iS10). The investigations of X-ray photoelectron spectroscopy (XPS) and UV photoelectron spectroscopy (UPS) were conducted using a Thermofisher ESCALAB Xi+ instrument with a monochromatic Al Kα X-ray and He-I resonance line ($h\nu$=21.22 eV), respectively. To conduct the depth-profile XPS analysis, the OSC film on the electrode-patterned wafer surface was etched to remove the surface OSC layer (e.g., gradually decrease the thickness of the OSC film) using an Ar2000 ion cluster beam with an etching rate of approximately 1.6 Å per second. The adhesion of the thin film is evaluated according to the standard ASTM test methods (ASTM D3359-09).[S3] The phases of the materials were identified using a RIGAKU TTRIII-18KW X-ray diffractometer equipped with a thin film attachment. The performance evaluation of the OFETs was conducted using a Keithley 4200 SCS semiconductor parametric analyzer under the default normal test mode. The field-effect mobility (μ_{FET}) of the OFETs was determined based on transfer curves using the following equation,

$$I_{DS} = (W/2L)\, C_i\, \mu_{FET}\, (V_{GS} - V_{TH})^2 \quad \text{(S1)}$$

Where, I_{DS} is the source-drain current, L and W respectively denote the length and width of the electrode channel, respectively. C_i denotes the real capacitance of SiO_2. V_{GS} and V_{TH} correspond to the gate voltage and threshold voltage, respectively.

2. Characterization on materials and devices

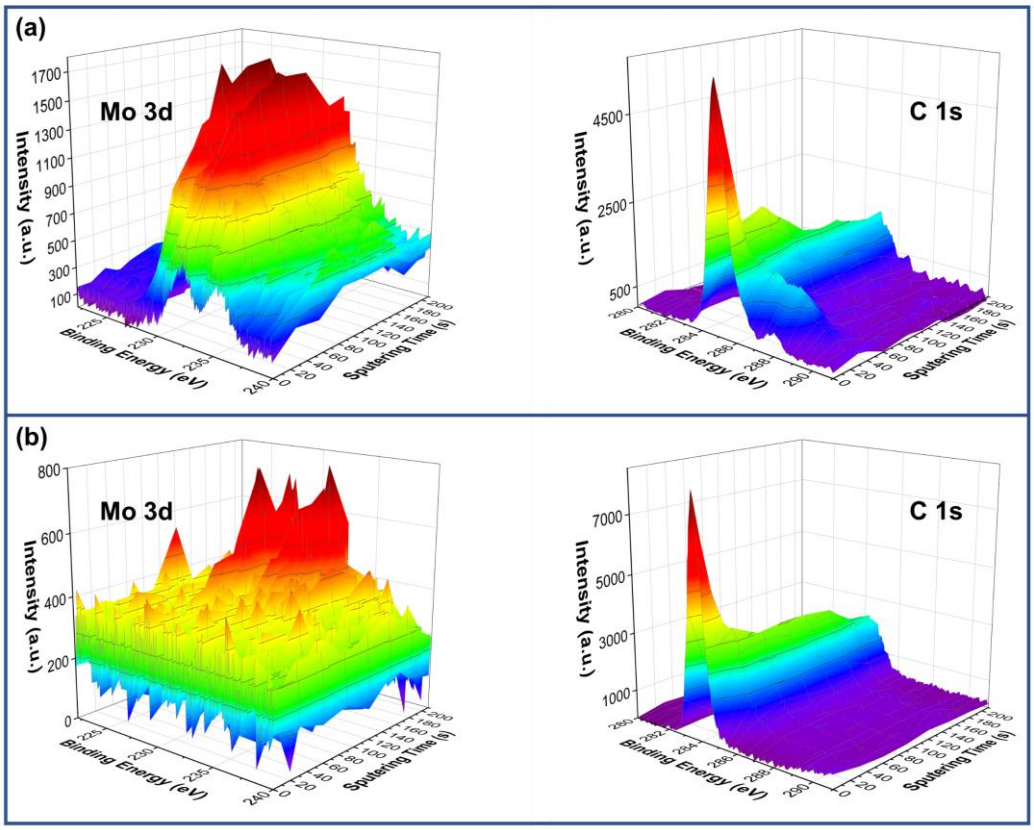

Figure S1. Depth-profile XPS analysis of element distribution of Mo (Mo 3p XPS spectra as shown in the left figure) and C (C 1s XPS spectra as shown in the right figure) in the OSC channels of OFETs: (a) BGBC/PVD-MoO_3@Au OFET and (b) BGBC/ECD-MoO_3@Au OFET. (An Ar ion cluster beam was applied to etch the OCS films to enable the recording of XPS data at different depth positions. The etching rate is approximately 1.6 Å per second.)

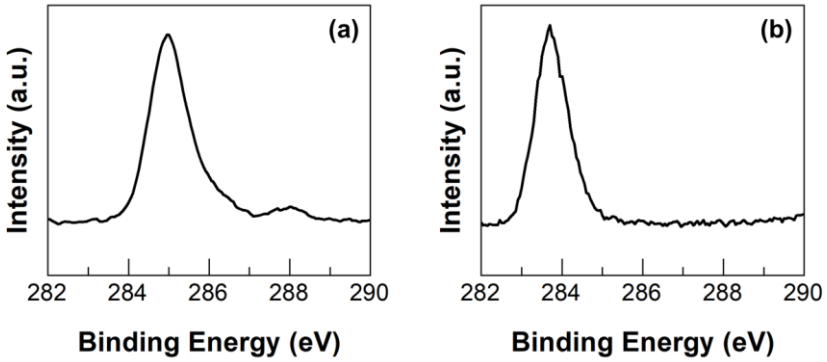

Figure S2. C 1s peak of the Rubrene films in the OFET channels of (a) BGBC/PVD-MoO_3@Au and (b) BGBC/ECD-MoO_3@Au devices.

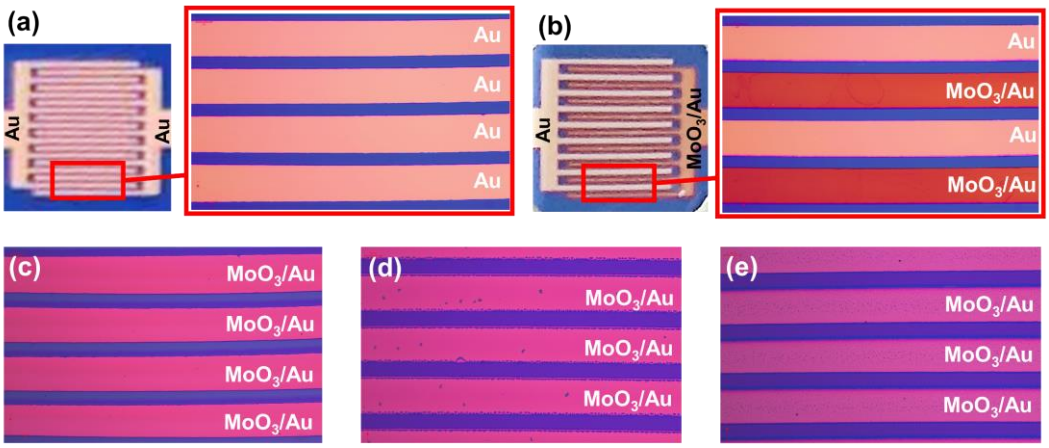

Figure S3. Optical images of (a) symmetric Au-based SDEs, (b) asymmetric Au/MoO_3-based SDEs fabricated by ECD method, (c) symmetric Au/MoO_3-based SDEs fabricated by PVD method, (d) symmetric Au/MoO_3-based SDEs fabricated by sol-gel method, and (e) symmetric Au/MoO_3-based SDEs fabricated by spray pyrolysis method, respectively.

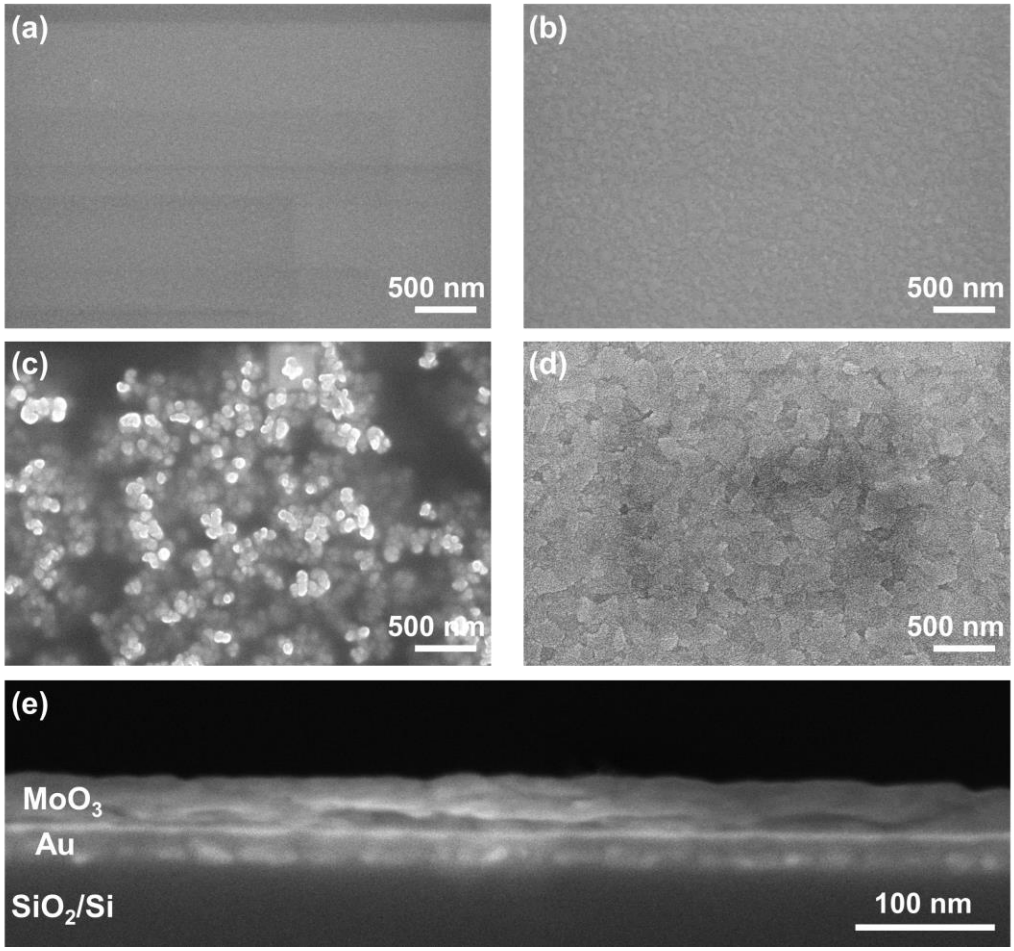

Figure S4. SEM image of (a) Au-electrode surface. SEM images of MoO_3-modified Au-electrode surface fabricated by (b) ECD method, (c) sol-gel method and (d) spray pyrolysis method, respectively. (e) A cross-section SEM image of ECD-MoO_3-modified Au electrode for device fabrication.

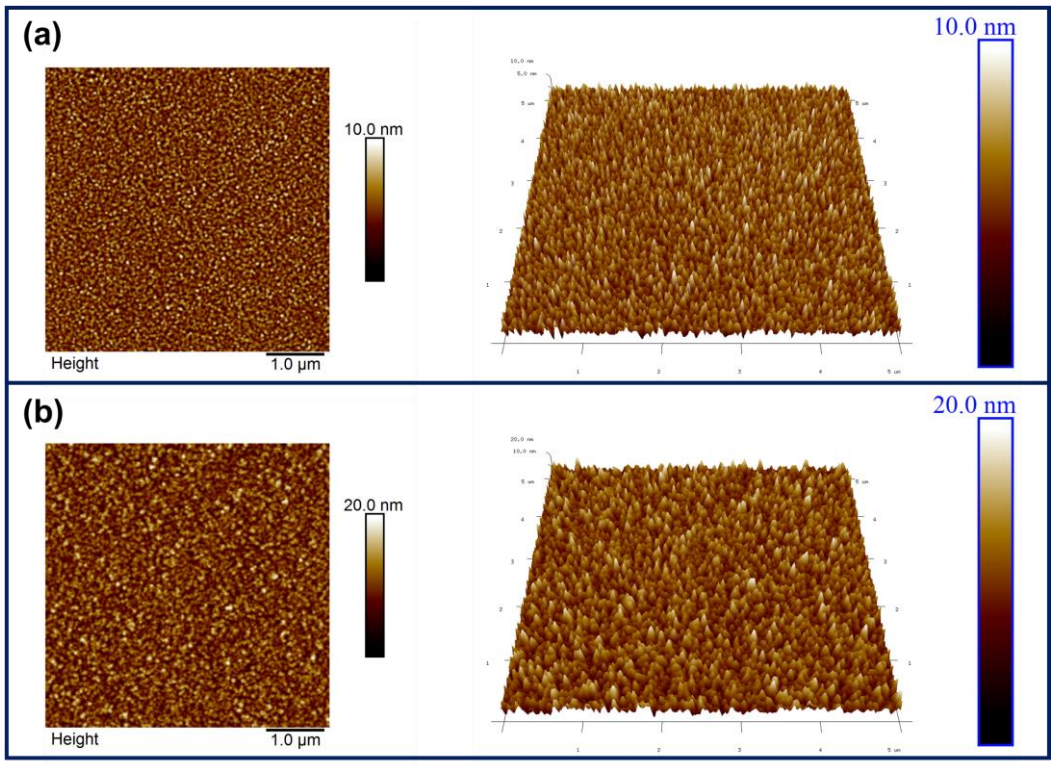

Figure S5. AFM surface morphologies of (a) Au electrode (R_a=1.02 nm) and (b) MoO_3-modified Au electrode (R_a=1.85 nm) fabricated by ECD method for device fabrication.

- **Evaluation of mechanical adhesion strength of MoO_3 layers**

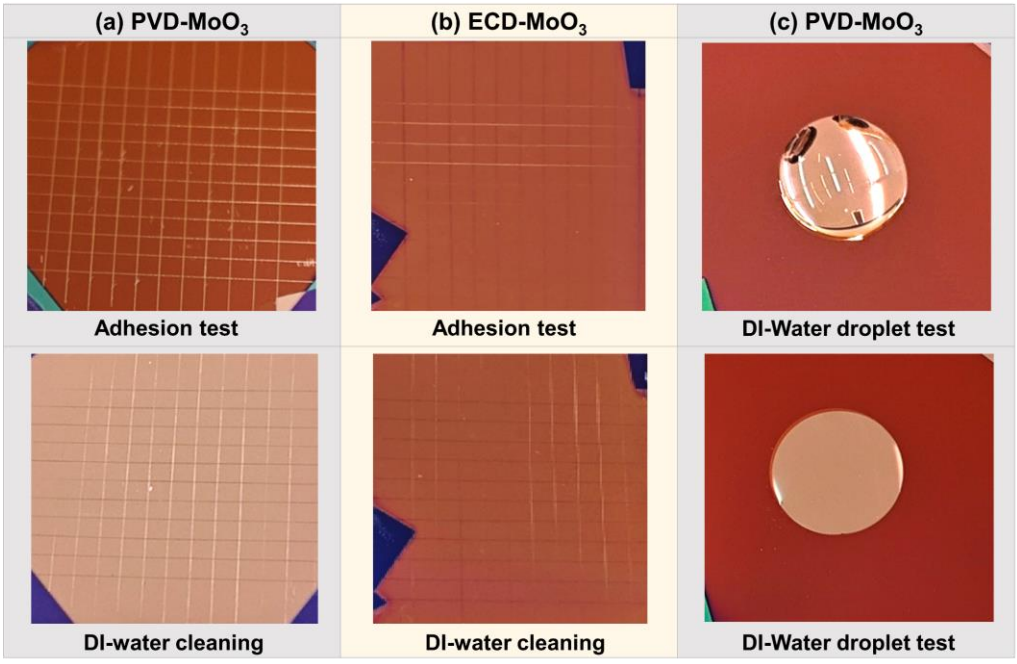

Figure S6. ASTM adhesion tests (as shown in the upper figures) and deionized water ultrasonic cleaning treatments (as shown in the lower figures) were carried out on (a) PVD-prepared and (b) ECD-prepared MoO_3 layers on Au-coated silicon substrates. (c) Schematic diagrams of deionized-water soak damaging PVD-prepared MoO_3 layers on Au-coated silicon substrates.

The adhesion of the MoO_3 thin-film layers was evaluated according to ASTM Standards (ASTM D3359-09).[S3] The MoO_3 layer deposited on a piece of the Au-coated Si/SiO_2 wafer was divided into a grid of 1.5 mm × 1.5 mm by means of a cross-cut tester blade. The 3M 600 tape, which is specifically designed for evaluating the adhesion of coatings on substrates, was pasted on the surface of the thin-film-coated substrate, and then peeled off from the substrate at a 90° angle to the substrate.

- As shown in **Figure S6a**, for the PVD-MoO_3 layer on the Au-coated silicon wafer surface, the detachment of small flakes of the MoO_3 layer at the intersection of the cuts and across-cut area is not greater than 5%. The adhesion strength of the PVD-MoO_3 layer on the Au-coated substrate is evaluated to ISO grade 1 (ASTM grade 4B) based on the standard of ISO 2409:2013(E).
- As shown in **Figure S6b**, for the ECD-MoO_3 layer on the Au-coated silicon wafer surface, the cut edges are completely smooth and there is no peeling at the grid edges. It indicates that the adhesion strength of the ECD-MoO_3 layer on the Au-coated substrate is very high, meeting the highest strength grade ISO grade 0 (ASTM grade 5B) based on the standard of ISO 2409:2013(E).

- **Evaluation of adhesion strength of MoO_3 layers for solution processing**

As shown in **Figures S6a**, subsequent to subjecting the MoO_3-coated wafers to ultrasonic treatment in deionized water (DI-water), the PVD-MoO_3 layer promptly and entirely detached from the wafer. The result indicates that the PVD-MoO_3 layer exhibits extremely inferior stability during solution processing. To distinguish whether the

damage of the PVD-MoO_3 layer is due to ultrasonic mechanical action or the surface tension effect of solutions, a DI-water droplet is dropped onto the PVD-MoO_3 layer. As shown in **Figure S6c**, the part of the PVD-MoO_3 layer in contact with the water drop immediately disperses and gets damaged. The results further indicate the PVD-MoO_3 layer cannot undergo the solution-based procedures for device fabrication.

For the ECD-MoO_3 layer, it can withstand ultrasonic treatment in deionized water without any observable damage, as shown in **Figure S6b**. It suggests the high adhesion strength of the ECD-MoO_3 layer and the potential of the ECD-MoO_3 modified electrodes for solution processing and device manufacturing in the industry.

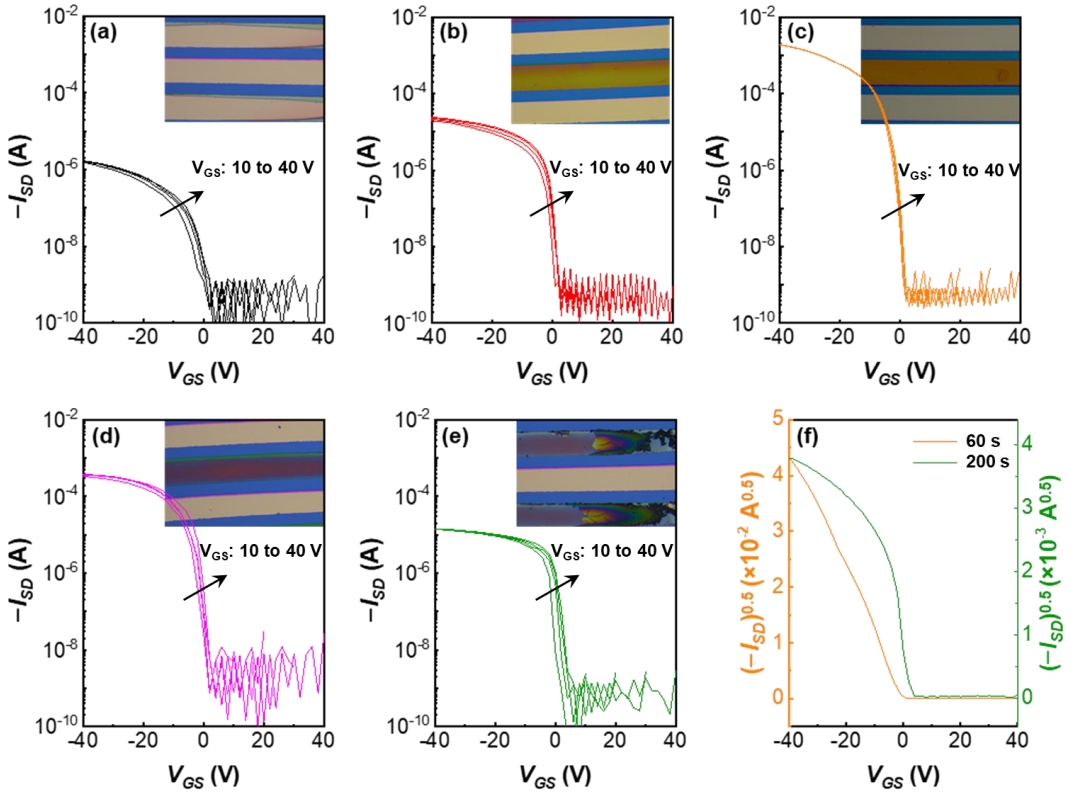

Figure S7. Transfer curves of Rubrene-based OFETs fabricated using the ECD-MoO_3@Au electrodes with different deposition durations of (a) 10, (b) 30, (c) 60, (d) 120, and (e) 200 seconds, respectively. (Insets show the optical images of the ECD-MoO_3@Au electrodes.) (f) Plots of $(-I_{SD})^{0.5}$ versus V_{GS} of OFETs with ECD-MoO_3 deposition durations of 60 second and 200 second.

To achieve the optimal device performance, the deposition duration of the ECD process is investigated to control the thickness and surface morphologies of the ECD-MoO_3 modification layers on the surface of Au electrodes. Under the deposition durations of 10, 30, 60, 120, and 200 seconds, the average thicknesses of the ECD-MoO_3 layer on the electrode surface are about 3.1, 27.6, 46.4, 60.7, and 69.1 nm, measured by a profilometer. Accordingly, the morphologies of these ECD-MoO_3 layers are shown in the insets in **Figures S7a-S7e**. As the ECD duration increases from 10 to 120 seconds, the coverage rate of the ECD-MoO_3 layers on the electrode surface increases, and the color of the ECD-MoO_3 layer becomes darker due to the increasing thickness. Based on the transfer curves of the devices fabricated using different thicknesses of ECD-MoO_3 layer for the electrode modification, it is evident that the modification of a uniform MoO_3 coverage on the electrode can effectively enhance the field-effect mobility of the devices and improve the operational stability by reducing electron injection into the p-type channel of the OFETs. With the increase in deposition duration, the thickness and coverage rate of the MoO_3 layer on the electrode surface are improved, and correspondingly, the performance of the device is also enhanced. A deposition duration of 60 seconds is optimal for attaining the best device performance. A deposition duration of 120 seconds is also acceptable for the formation of uniform ECD-MoO_3 layer for the device fabrication. However, it should be noted that an excessively thick film impacts carrier transport at the OSC/electrode surface, which results in a slight decrease in device performance. When the ECD duration is further extended to 200 seconds, the ECD-MoO_3 layer peels off from the electrode surface,

leading to an uneven electrode surface. As a result, the performance of the device is degraded. **Figure S7f** plots the $(-I_{SD})^{0.5}$ as a function of V_{GS} for the OFETs with ECD-MoO_3 deposition durations of 60 and 200 seconds. It is evident that the device subjected to a ECD process for 60 seconds demonstrates the ideal operation characteristics of a transistor, in which $(-I_{SD})^{0.5}$ has linear a function in relation to V_{GS}. However, the device undergoing a ECD process for 200 seconds that exhibits a non-linear relationship. It is because the non-uniform contact between the modified electrode and the OSC film, leading to the non-ideal transistor characteristics. According to these results, the electrode modified by the ECD process for 60 seconds was selected in this work for further study.

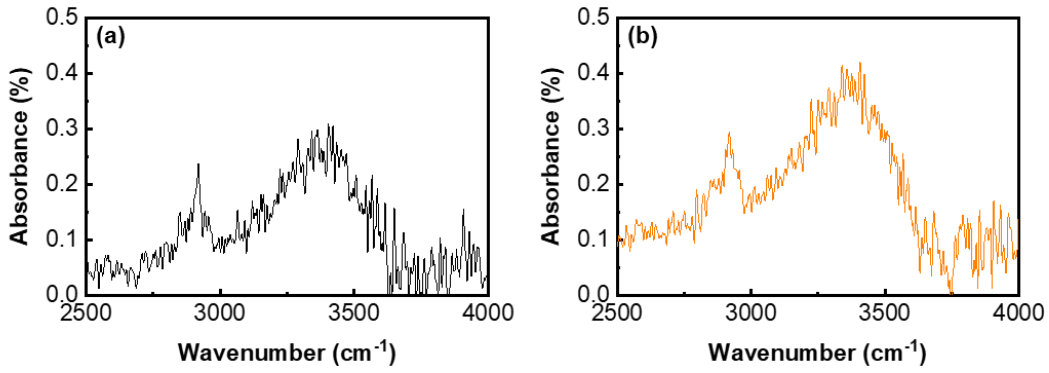

Figure S8. FTIR spectra of (a) Au electrodes and (b) ECD-MoO_3@Au electrodes on Si/SiO_2 wafers.

Before the FTIR measurement, the samples underwent a surface cleaning treatment, which is the same as the pre-procedure applied for the fabrication of OFET devices. The samples were sequentially subjected to ultrasonic cleaning with acetone, methanol, and deionized water, followed by baking in air at 100 °C for 10 min and ultraviolet ozone treatment for 30 min. It can be seen that both samples demonstrate an extremely low absorption of less than 0.5% within the range of 2500 to 3700 cm^{-1},

indicating that there are merely trace amounts of hydroxyl groups on the surfaces. These trace amounts of hydroxyl groups are insufficient to exert a significant impact on the device performance of the OFETs.

To further verify the influence of hydroxyl groups and potentially surface-adsorbed water, the wafer patterned with ECD-MoO_3@Au electrode was annealed at 450 °C for 2 hours in a muffle furnace under an air atmosphere, followed by the fabrication of the Rubrene-based OFET. **Figure S9** presents the transfer curves of the device. Evidently, the device performance was not improved. Therefore, the potentially trace residual hydroxyl groups and adsorbed water molecules have a negligible effect on the device performance of the OFET. It is worth noting that the device performance appears to have deteriorated in this annealing case. This is attributed to the fact that after the annealing treatment, the wafer was not re-cleaned by ultrasonic cleaning in solvents in order to prevent the introduction of new hydroxyl groups or water. Consequently, the possible contaminants on the wafer surface during the sample transfer process might have led to the decline in device performance.

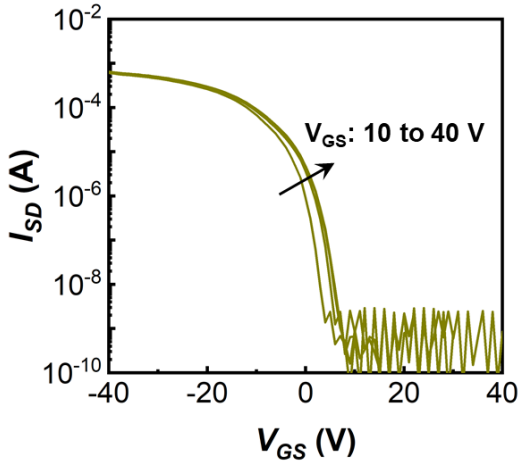

Figure S9. Transfer curve of Rubrene-based OFET fabricated using high-temperature annealed ECD-MoO_3@Au electrodes.

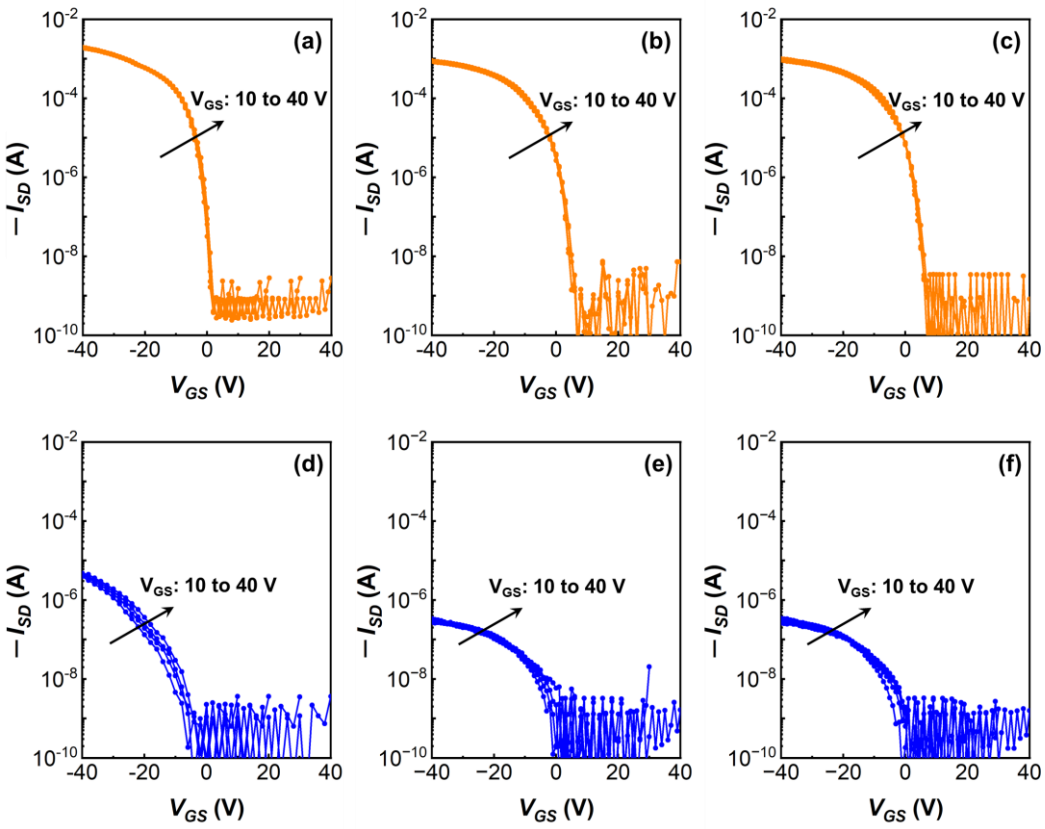

Figure S10. Transfer curves of Rubrene-based OFETs fabricated in three batches: (a-c) BGBC/ECD-MoO_3@Au OFETs and (d-f) BGBC/Au OFETs.

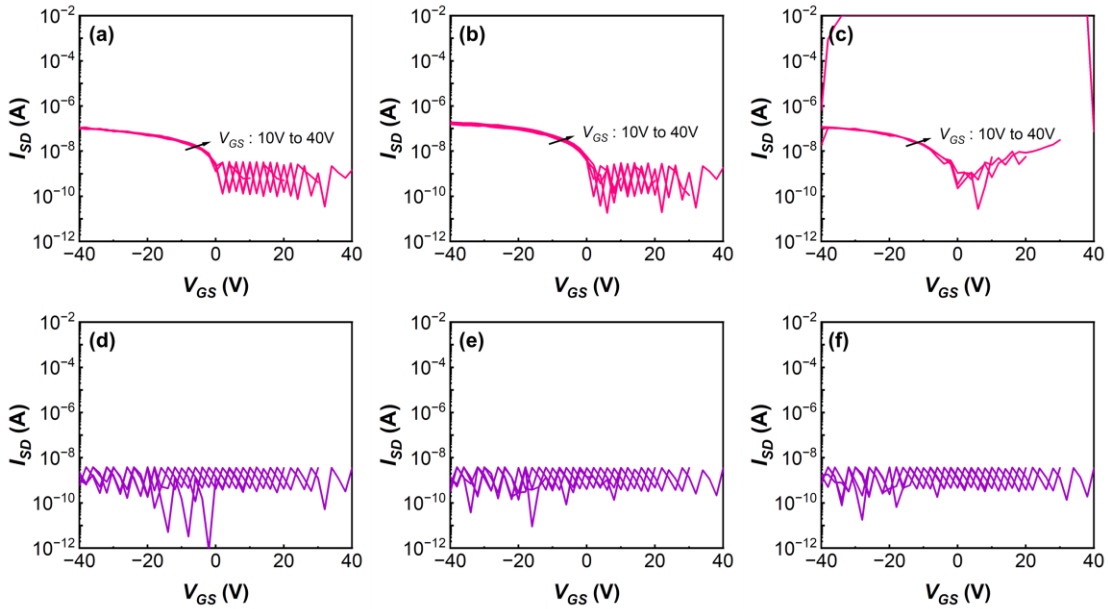

Figure S11. Transfer curves of Rubrene-based OFETs fabricated using MoO_3-modified source-drain electrodes by (a-c) sol-gel spin-coating method and (d-f) spray pyrolysis method.

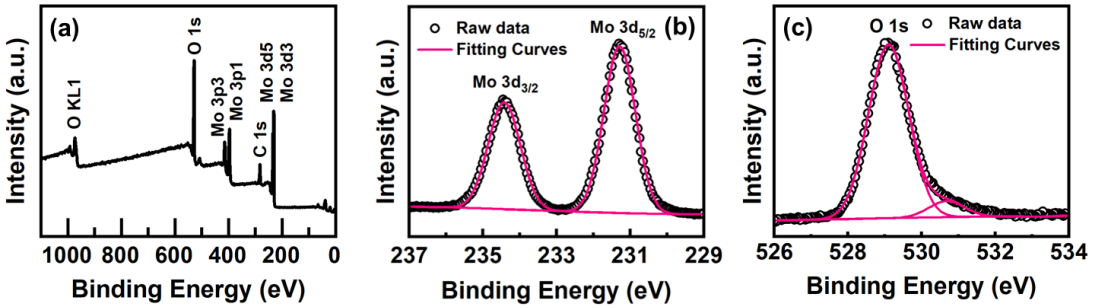

Figure S12. (a) Full-scan XPS spectrum, (b) Mo 3d XPS spectrum and (c) O 1s XPS spectrum of ECD-MoO_3 layer.

Figure S12a shows the XPS spectrum of the ECD-MoO_3 layer deposited on the Au-coated silicon wafer. There is no impurity element in the ECD-MoO_3 layer. The Mo 3d XPS spectrum (**Figure S12b**) exhibits symmetric Gaussian peaks at 231.4 eV and 234.2 eV, in which are assigned to the Mo 3d5/2 and 3d3/2 spin-orbit components of Mo^{6+} cations, respectively.[S4] The O 1s XPS spectrum (**Figure S12c**) exhibits a Gaussian peak at 529.1 eV and a shoulder peak at 530.8 eV, which are attributed to lattice oxygen and oxygen coordinated with molybdenum cations in low oxidation states, respectively.[S5] The weak shoulder peak indicates the ECD- MoO_3 layer is close to the stoichiometric ratio with minimal anion deficiency.

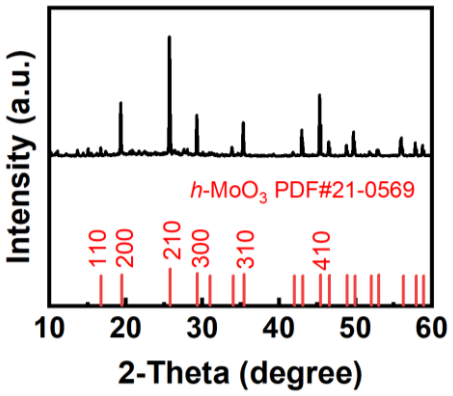

Figure S13. XRD spectrum of ECD-MoO_3 layer. The sharp diffraction peaks indicate the high crystallinity of ECD-MoO_3 layer, which belongs to hexagonal MoO_3 phase (JCPDS card no. 21-0569).

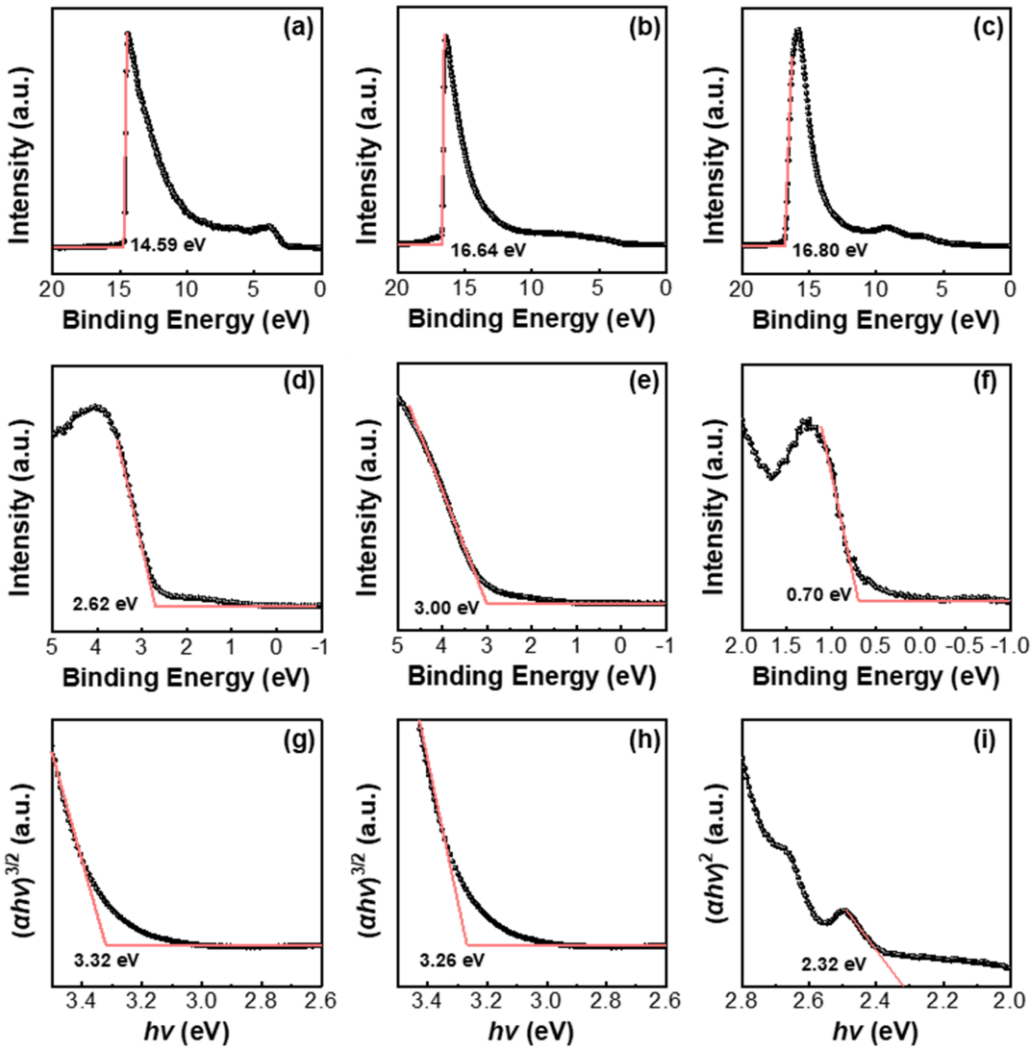

Figure S14. Full-scan XPS spectra of (a) ECD-MoO_3, (b) PVD-MoO_3, and (c) Rubrene film. Valence band spectra of (d) ECD-MoO_3, (e) PVD-MoO_3, and (f) Rubrene film. UV-vis absorption spectra of (g) ECD-MoO_3, (g) PVD-MoO_3, and (i) Rubrene film. (The work functions measured by the photoelectron spectrometer are calibrated against the value of 5.10 eV for Au.)

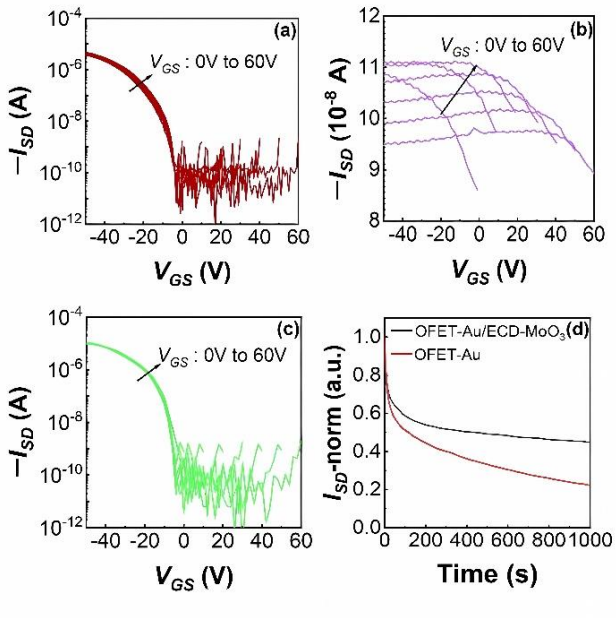

Figure S15. Transfer curves of TIPS-pentacene-based BGBC OFETs (V_{SD} = −50 V): (a) BGBC/Au, (b) BGBC/PVD-MoO_3@Au, (c) BGBC/ECD-MoO_3@Au. (d) Bias-stress stability test of TIPS-pentacene-based BGBC/Au (Red line) and BGBC/ECD-MoO_3@Au (Black line) OFETs at a DC voltage bias of V_{GS} = −50 V and V_{SD} = −50 V.

References:

[S1] Kaya K K, Orak C, Horoz S. Enhancing the performance of dye-sensitized solar cells (DSSCs) through Mn and Ni doping of MoO_3 thin films. ***Journal of the Australian Ceramic Society***, 2025, 61, 2005-2017.

[S2] Chandoul F, Boukhachem A, Hosni F, et al. Change of the properties of nanostructured MoO_3 thin films using gamma-ray irradiation. ***Ceramics International***, 2018, 44(11): 12483-12490.

[S3] Hamm E, Reis P, LeBlanc M, et al. Tearing as a test for mechanical characterization of thin adhesive films. ***Nature materials***, 2008, 7(5): 386-390.

[S4] Baishya R, Roy K, Das S K. High-rate performance of H_xMoO_3 for aqueous aluminium-ion batteries. ***Chemical Communications***, 2025, 61(44): 8031-8034.

[S5] Bhardwaj S, Santra S, Dey R S. Controlled nucleation of ultrasmall MoO_3 nanoparticles on defective graphene for enhanced ammonia efficiency. **Chemical Communications**, 2024, 60(94): 13959-13962.